

**Hydroxyl-functionalized poly(trimethylene carbonate)  
electrolytes for 3D-electrode configurations**

Journal:	<i>Polymer Chemistry</i>
Manuscript ID:	PY-ART-03-2015-000446.R1
Article Type:	Paper
Date Submitted by the Author:	18-May-2015
Complete List of Authors:	Mindemark, Jonas; Uppsala University, Department of Chemistry - Ångström Laboratory Sun, Bing; Uppsala University, Department of Chemistry - Ångström Laboratory Brandell, Daniel; Uppsala University, Department of Chemistry - Ångström Laboratory



Journal Name

ARTICLE

## Hydroxyl-functionalized poly(trimethylene carbonate) electrolytes for 3D-electrode configurations

J. Mindemark,\* B. Sun and D. Brandell

Received 00th January 20xx,  
Accepted 00th January 20xx

DOI: 10.1039/x0xx00000x

[www.rsc.org/](http://www.rsc.org/)

Polymer electrolytes were prepared from an aliphatic polycarbonate with 10 mol% of repeating units having a hydroxyl-functional side group, with added LiTFSI salt. The hydrogen bond-interacting side groups were found to be beneficial for improving adhesion to 2D planar electrode material surfaces. These favorable surface properties proved to be valid also for 3D-structured systems since thin, conformal coatings could be cast on 3D-microstructured electrodes. In addition, the electrolytes were found to have reasonable ionic conductivity (up to  $2.7 \times 10^{-8} \text{ S cm}^{-1}$  at 25 °C and  $2.3 \times 10^{-6} \text{ S cm}^{-1}$  at 60 °C) that was almost independent on salt concentration. This demonstrates how a hydroxyl-functional polymer approach is suitable for creating 3D-structured electrode–electrolyte assemblies for microbattery applications.

### Introduction

Current Li-ion battery technology is largely aimed towards powering portable electronics with much of the research effort directed towards up-scaling for electric vehicles and large-scale energy storage.<sup>1, 2</sup> In these applications, gravimetric and volumetric energy and power densities are key performance indicators. At the other end of the scale, miniaturization of batteries presents a considerable challenge. Such microbatteries would be of tremendous utility for powering a vast and diverse array of microscale devices brought forth by recent developments in microelectromechanical systems (MEMS) technology,<sup>3</sup> where a large *capacity per footprint area* is required. This would be possible to achieve in combination with reasonable power performance by a 3D-architected Li-ion microbattery.<sup>4</sup>

In any conventional battery design, there is a trade-off between power and energy density. High capacity can be obtained by having electrodes composed of thick layers of active material but, as sluggish solid-state diffusion will limit the kinetics of lithiation and delithiation, such a ‘thick-film’ battery will have low attainable specific power. High power density is instead favored by thin-film designs which offer short intra- and interelectrode ion diffusion paths. In current Li-ion battery designs, a compromise is reached by having the active material in particulate form, thus enabling the preparation of relatively thick, porous electrodes while minimizing the dependence on slow solid-state diffusion. One could argue that such a strategy entails a certain level of 3D

structuring of the electrodes; however, the full battery geometry is still largely two-dimensional.

For microbatteries, a more efficient capacity/power compromise would be possible in a truly 3D-structured battery. This entails electrodes with complementary 3D-architecturing, separated by a thin electrolyte membrane that minimizes ion diffusion distances throughout the cell. While a wide variety of 3D-microstructured electrodes with different designs can be produced,<sup>5, 6</sup> the development of 3D-microbatteries is largely limited by the challenge posed by the need to find a suitable electrolyte.<sup>4, 5, 7</sup> Essential for 3D-microbatteries is a thin, conformal, robust, pinhole-free electrolyte layer that can also act as a physical separator between the electrodes during assembly and operation, and still be flexible enough to accommodate volume changes in the electrodes during charge/discharge.<sup>4, 8</sup> To this end, solid polymer electrolytes (SPEs) are suitable candidates. Whereas in a macroscopic battery SPEs typically offer too low ionic conductivities to be of practical use,<sup>2</sup> on a much smaller scale – equivalent to short diffusion distances – good performance can be achieved even at modest levels of ionic conductivity.<sup>5</sup> Furthermore, polymer electrolytes offer additional benefits such as low cost, safe operation, mechanical flexibility, easy processing through solvent casting and a potentially more uniform current distribution compared to liquid electrolytes.<sup>5, 9, 10</sup>

However, applying a thin, conformal coating of an ionically conducting polymer to a complex 3D-structured substrate is far from trivial and several different strategies for achieving this have been presented. Rhodes *et al.* investigated nanoscale solid polymer networks of poly(phenylene oxide) (PPO) electrodeposited on MnO<sub>x</sub> ambigel films and demonstrated highly electronically insulating properties in 15 nm thick polymer layers.<sup>7</sup> El-Enany *et al.* used electropolymerization to deposit a thin film of poly(acrylonitrile) directly onto 3D-

Department of Chemistry – Ångström Laboratory, Uppsala University Box 538, SE-751 21 Uppsala. E-mail: jonas.mindemark@kemi.uu.se

Electronic Supplementary Information (ESI) available: Additional figures showing schematic ion–polymer interactions as well as SEM micrographs of pristine nanostructured substrates. See DOI: 10.1039/x0xx00000x

structured electrode surfaces.<sup>11</sup> While the resulting films were brittle when dry, soaking in a traditional liquid electrolyte softened the polymer layer and provided the necessary ionic conductivity while still allowing cell assembly with a stable open circuit voltage. Electropolymerization was also used by Sun *et al.* to produce micrometer-thin electrolyte films of polymerized poly(propylene glycol) diacrylate on a 3D-substrate of Cu<sub>2</sub>O-coated Cu nanopillars.<sup>12</sup> While having the advantages of being surface-initiated and producing a film covalently grafted to the surface in a self-limiting growth process, electropolymerization or electrografting is largely limited to redox- or free radical-polymerizable monomers.<sup>13, 14</sup> A more general approach was used by Tan *et al.*, who used an oligomeric poly(ether amine) with surfactant properties in electrolyte formulations in order to obtain thin conformal coatings of UV-crosslinkable poly(propylene glycol) diacrylate on LiFePO<sub>4</sub> particles as well as on Cu and Cu<sub>2</sub>Sb nanopillars.<sup>15–17</sup> While no truly three-dimensional cells were assembled, the polymer-coated electrodes showed decent device performance in lithium half-cells at 60 °C. Later, Sun *et al.* introduced crosslinkable methacrylate end-groups to the same poly(ether amine) to combine the functionalities of the two components in a single bifunctional macromonomer that could be coated conformally onto LiFePO<sub>4</sub> particles and cycled in half-cells at 60 °C.<sup>18</sup> This approach of utilizing functional groups that can interact with the electrode surfaces by means of hydrogen bonding offers more flexibility as it can be applied to a large variety of polymer systems in macromonomers, high-molecular-weight polymers or even at the monomer stage. We have previously demonstrated the potential of using polycarbonate-based electrolytes in Li-ion batteries.<sup>19–21</sup> Since the versatile chemistry of the six-membered cyclic carbonate monomer platform lends itself well for synthesizing polymers with specific and diverse functionalities,<sup>22–27</sup> this potential naturally extends to functional 3D-microbattery electrolytes. In the present paper, we demonstrate how this strategy can be applied to polycarbonates to obtain polymer electrolytes for 3D-microbatteries by introducing hydroxyl functionalities in an aliphatic polycarbonate backbone.

## Experimental

### Materials

High-molecular-weight poly(trimethylene carbonate) (PTMC) was synthesized as described elsewhere.<sup>19</sup> The polymer  $M_n$  was determined by GPC to 457 000 g/mol with PDI = 1.27. Trimethylene carbonate (TMC; Boehringer Ingelheim) was handled and stored in a glovebox and used as received. Lithium bis(trifluoromethanesulfonate) (LiTFSI; Purolite, Ferro Corporation) was dried under vacuum at 120 °C for 24 h. Amberlyst 15 ion-exchange resin (Aldrich) was washed with acetone before use. Dry dichloromethane (DCM; Fisher Scientific) was obtained by storing over 4 Å molecular sieves. Stannous 2-ethylhexanoate (Sn(Oct)<sub>2</sub>; Sigma) was used as a 1 M solution in anhydrous toluene (Acros Organics). All other

chemicals were obtained from commercial sources and used without further purification.

### Instrumentation and general considerations

<sup>1</sup>H NMR spectra were acquired using a JEOL Eclipse+ 400 MHz NMR spectrometer. Coupling constants are given in Hz. Thermal properties were measured using differential scanning calorimetry on a TA Instruments DSC Q2000. Samples were hermetically sealed in aluminum pans and cooled at a rate of 5 °C/min to –40 °C followed by heating at 10 °C/min to 130 °C for measurement. Scanning electron microscopy imaging was performed on a Zeiss Merlin SEM with a working distance of about 8 mm under a probe current of 80 µA and 5 keV. GPC data was recorded on a Verotech PL-GPC 50 equipped with a refractive index detector and two PolarGel-M organic GPC columns. Chloroform was used as the eluent at a flow rate of 1 ml/min and the system was calibrated against narrow polystyrene standards.

### Synthesis of (2,2,5-trimethyl-1,3-dioxan-5-yl)methanol

90 g (0.75 mol) of 1,1,1-tris(hydroxymethyl)ethane was dissolved in 400 mL of acetone and 1 g of Amberlyst 15 acidic ion-exchange resin was added. The mixture was left to react under stirring for 14 h. The ion-exchange resin was filtered off and the solvent was evaporated. Distillation under reduced pressure afforded the title compound (63.4 g, 53%), bp 99–100 °C/8 mbar, as a colorless, viscous liquid. <sup>1</sup>H NMR  $\delta_H$  (400 MHz; DMSO-d<sub>6</sub>) 0.75 (3 H, s, Me), 1.27 (3 H, s, Me), 1.33 (3H, s, Me), 3.39 (2 H, br d,  $J$  = 5.5 Hz, CH<sub>2</sub>OH), 3.43 (2 H, d,  $J$  = 11.7 Hz, CH<sub>2</sub>O), 3.56 (2 H, d,  $J$  = 11.7 Hz, CH<sub>2</sub>O), 4.49 (1 H t,  $J$  = 5.5 Hz, OH).

### Synthesis of 2-benzyloxymethyl-2-methyl-1,3-propanediol

To a mixture of 24 g (0.15 mol) of (2,2,5-trimethyl-1,3-dioxan-5-yl)methanol, 8.1 g (25 mmol) of tetrabutylammonium bromide (TBAB) and 18 ml (0.15 mol) of benzyl bromide was added 20 g (0.36 mol) of freshly ground KOH. The mixture was allowed to react under stirring and heating in a 40 °C oil bath for 10 h. The reaction was quenched by addition of 100 ml of deionized water and the mixture was extracted with 300 ml of diethyl ether. The ether phase was washed with 2×100 ml of deionized water and 100 ml of brine before the solvent was evaporated. The remainder was dissolved in a mixture of 100 ml of THF and 100 ml of 1 M aqueous HCl and refluxed for 9 h. The solution was carefully neutralized by addition of 100 ml of saturated aqueous NaHCO<sub>3</sub> and extracted with 2×200 ml of ethyl acetate. The organic phases were combined, dried with sodium sulfate, filtered and evaporated. The product was recrystallized from toluene, washed with hexane and dried under vacuum to yield 21.5 g (68%) of 2-benzyloxymethyl-2-methyl-1,3-propanediol as a slightly yellowish solid. <sup>1</sup>H NMR  $\delta_H$  (400 MHz; DMSO-d<sub>6</sub>) 0.80 (3 H, s, Me), 3.27 (2 H, s, CH<sub>2</sub>O), 3.28 (4 H, br d,  $J$  = 5.5 Hz, CH<sub>2</sub>OH), 4.31 (2H, t,  $J$  = 5.5 Hz, OH), 4.44 (2 H, s, CH<sub>2</sub>O), 7.24–7.37 (5 H, m, Ph).

### Synthesis of 2-benzyloxymethyl-2-methyltrimethylene carbonate (BMC)

12.6 g (60.0 mmol) of 2-benzyloxymethyl-2-methyl-1,3-propanediol was dissolved in 160 ml of dry DCM. To this solution was added, gradually over the course of 30 min, 11.7 g (72 mmol) of 1,1'-carbonyldiimidazole (CDI). The resulting solution was immediately washed with 2×160 ml of 1 M hydrochloric acid and 160 ml of saturated aqueous NaHCO<sub>3</sub>. The organic phase was separated, dried with MgSO<sub>4</sub> and the solvent was evaporated. The crude product was recrystallized from THF/diethyl ether to yield the cyclic carbonate (6.37 g, 45%) as a colorless solid. <sup>1</sup>H NMR δ<sub>H</sub> (400 MHz; CDCl<sub>3</sub>: 1.11 (3 H, s, Me), 3.41 (2 H, s, CH<sub>2</sub>O), 4.08 (2 H, BB' of AA'BB', CH<sub>2</sub>O), 4.36 (2 H, AA' of AA'BB', CH<sub>2</sub>O), 4.53 (2 H, s, CH<sub>2</sub>O), 7.28–7.38 (5 H, m, Ph).

#### Synthesis of poly(TMC-co-BMC)

In a glove box under Ar, an oven-dried stainless steel reactor was charged with 4.59 g (45 mmol) of TMC and 1.18 g (5 mmol, 10%) of BMC. 0.01 mmol of Sn(Oct)<sub>2</sub> was added as a 10 μl of a 1 M solution in anhydrous toluene. The reactor was sealed and heated in a 130 °C oven for 3 days. Following melting of the monomers, the reactor was shaken regularly during the initial few hours to ensure proper mixing. After allowing the reactor to cool down and the slightly amber-colored rubbery contents were discharged inside the glove box and used without further purification.  $M_n$  (GPC): 329 000 g/mol, PDI = 1.38.

#### Deprotection of poly(TMC-co-BMC)

3.3 g of the benzyl ether-protected poly(TMC-co-BMC) was dissolved in 150 ml of a 3:1 mixture of DCM and MeOH and 300 mg of 5% Pd/C was added. The reaction vessel was purged first with Ar, then with H<sub>2</sub> and finally pressurized with H<sub>2</sub> to 0.4 MPa (60 psi). The reaction was allowed to proceed under stirring for 26 h. The reaction mixture was filtered through Celite, washing the Celite pad with additional 3:1 DCM/MeOH, and the resulting solution was concentrated through rotational evaporation. 150 ml of DCM was added to dissolve the polymer and the resulting solution was further filtered through a 0.45 μm PTFE syringe filter before precipitating the polymer in MeOH. After decanting the solvent, the polymer was dried at ~37 °C in a vacuum oven over P<sub>2</sub>O<sub>5</sub>. Yield: 2.28 g of hydroxyl-functional PTMC, referred to as PTMC-OH, as a colorless, transparent rubbery solid.  $M_n$  (GPC): 271 000 g/mol, PDI = 1.37.

#### Electrolyte preparation

Polymer electrolytes were prepared and stored in an Ar-filled glove box to prevent moisture contamination. Solutions of controlled ratios of PTMC-OH and LiTFSI in anhydrous acetonitrile were cast in PTFE molds. The solvent was evaporated using a vacuum oven setup inside the glove box; the pressure was decreased from an initial 200 mbar to full vacuum (<1 mbar) at room temperature during 20 h followed by heating at 60 °C under full vacuum for 40 h. Circular samples with a diameter of 14 mm were punched from the resulting films. Electrolytes are identified as PTMC-OH<sub>*n*</sub>LiTFSI, where *n* refers to the [carbonate]:[Li<sup>+</sup>] ratio.

#### Ionic conductivity

The total ionic conductivity of the electrolytes was obtained through electrochemical impedance spectroscopy. Polymer electrolyte films were sandwiched between stainless steel blocking electrodes and sealed in Swagelok-type cells. The temperature was measured using a thermocouple positioned a few mm from one of the electrodes and the cells were heated in an oven to 100 °C. Following annealing for 1 h at 100 °C to improve interfacial contacts, measurements were performed at regular temperature intervals during cooling to 25 °C using a Schlumberger Impedance/Gain-phase Analyzer SI 1260 between 1 Hz–1 MHz at an amplitude of 10 mV. The bulk ionic resistance was obtained as the low-frequency x-axis intercept of the semicircle in the Nyquist plot.

#### Scratch testing

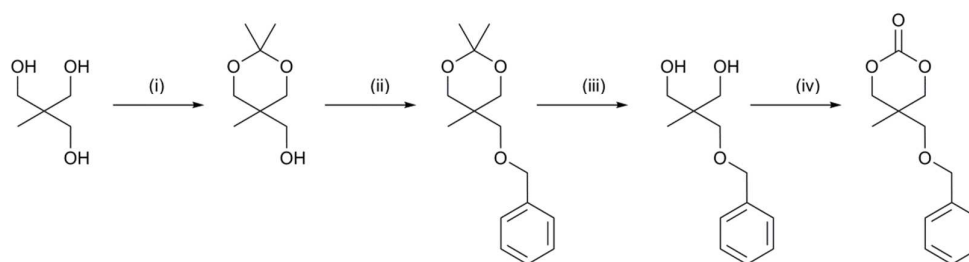
Planar substrates of Ti and Cu were polished and oxidized thermally in air to form TiO<sub>2</sub> (400 °C, 4 h) and Cu<sub>2</sub>O, respectively (150 °C, 4 h). Thin films of PTMC and PTMC-OH were deposited on the substrates through solvent casting from an acetonitrile solution. The coated substrates were dried at 50 °C for 5 h in a vacuum oven. The adhesion of the films was assessed through scratch testing using a CSEM REVETEST, ramping the load from 0 to 30 N at a rate of 30 N/mm and a speed of 10 mm/min. A 200 μm standard Rockwell tip was used and the adhesion of the polymer layer was evaluated through SEM imaging.

#### Morphological analyses on 3D substrates

Morphological analysis was performed by applying a solution of PTMC-OH<sub>8</sub>LiTFSI in acetonitrile on 3D electrode substrates, *i.e.*, LiFePO<sub>4</sub>-coated ultraporous carbon foam and Cu<sub>2</sub>O-nanopillars. The preparation of 3D-electrodes can be found described elsewhere.<sup>28, 29</sup> The solvent was evaporated in a vacuum oven at 55 °C for 6 h. All preparations were performed in an argon-filled glove box. The morphology was imaged using SEM.

## Results and Discussion

The ability of hydrogen bond-induced formation of thin, conformal coatings on electrode active material particles has been demonstrated using oligomeric poly(ether amine)s by Sisbandini *et al.*<sup>30, 31</sup> The same strategy has later been used to prepare conformal polymer electrolyte films on complex electrode substrates.<sup>15, 17, 18</sup> This is a simple, promising strategy that should be possible to extend to polycarbonate electrolytes as well. However, while previous work has relied on hydrogen bond interactions between the primary amine end-groups of the oligoether and the inorganic electrode surface, amines are not suitable functionalities in a polycarbonate context because of the reactivity of carbonates, particularly the six-membered cyclic monomers, with amines to form carbamates.<sup>32, 33</sup> This turned our attention towards other hydrogen bond-forming moieties. In the context of aliphatic polycarbonates, carboxylic acids and hydroxyls are obvious choices that can be easily introduced as functional side groups at the monomer level using a benzyl ester/ether protecting group strategy to avoid branching during



Scheme 1. Synthesis of the BMC monomer. Reaction conditions: (i) acetone, Amberlyst 15, r.t.; (ii) benzyl bromide, KOH, TBAB, 40 °C; (iii) THF, HCl, H<sub>2</sub>O, reflux; (iv) Cl, DCM, r.t.

polymerization.<sup>34–37</sup> Post-polymerization deprotection through catalytic hydrogenation then gives the functional polymer. The benzyl ester functionality, however, is prone to transesterification reactions during polymerization, particularly at high molecular weight and/or high conversion. This can potentially lead to uncontrolled crosslinking, thus rendering the resulting polymer insoluble and unsuitable for further processing.<sup>35</sup> The presence of this detrimental side reaction was confirmed in preliminary experiments with a benzyl ester-functional cyclic carbonate monomer and it was concluded that polymers containing this functionality would be limited to low molecular weights. Since a molecular weight in excess of 100 000 g/mol is necessary for mechanical stability in the absence of (controlled) crosslinking,<sup>38</sup> this route was abandoned in favor of hydroxyl functionalities.

For the preparation of high-molecular-weight polycarbonates with hydroxyl side groups, the benzyl ether-functional

monomer 2-benzoyloxymethyl-2-methyltrimethylene carbonate (BMC) was synthesized as shown in Scheme 1. The same monomer has previously been synthesized by Darenbourg *et al.* through a different route, starting from diethyl methylmalonate.<sup>39</sup> Analogous to the previously published synthesis of the cyclic monomer 2-heptyloxymethyl-2-ethyltrimethylene carbonate,<sup>21</sup> the present synthesis instead starts from a commercially available triol and proceeds through acetonide protection/deprotection in four steps ending with ring-closing of the benzyl ether-functional 1,3-propanediol derivative with 1,1'-carbonyldiimidazole. The BMC monomer was copolymerized with trimethylene carbonate (TMC) using stannous 2-ethylhexanoate (Sn(Oct)<sub>2</sub>) as a polymerization catalyst to yield a copolymer with 10% of the benzyl ether-functional monomer. The copolymer was deprotected using palladium-catalyzed hydrogenolysis to yield a hydroxyl-functional polycarbonate (PTMC-OH). The structure

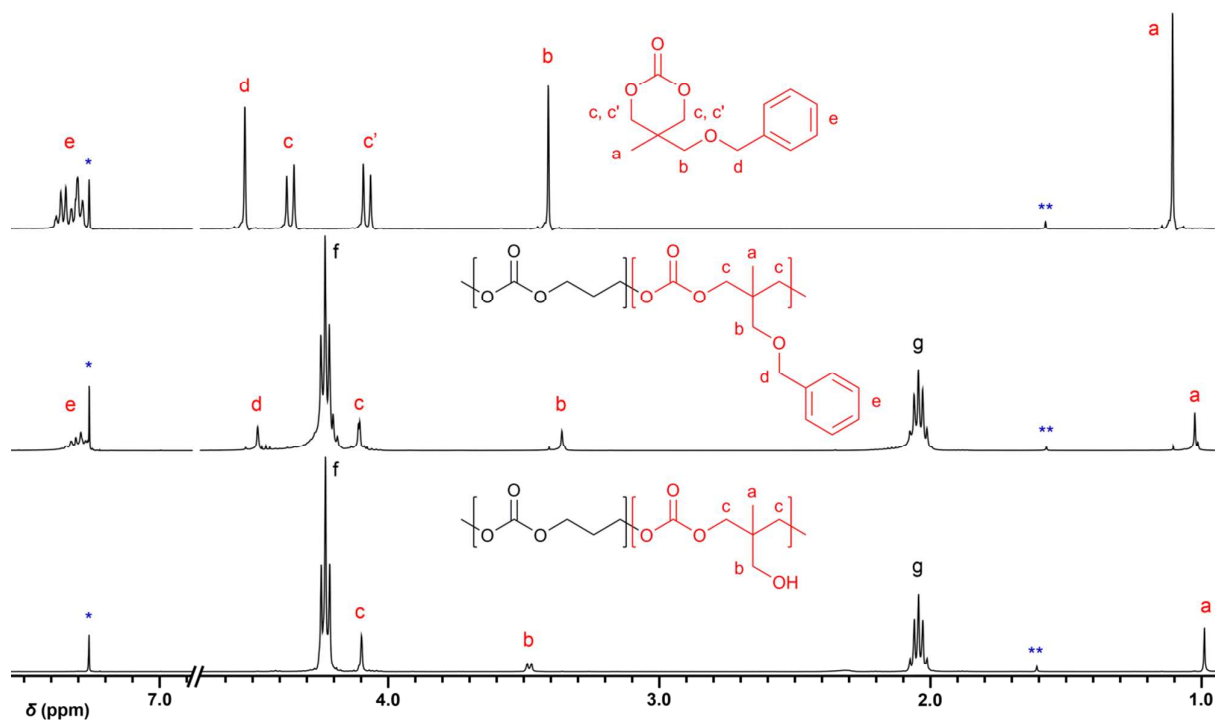


Figure 1. <sup>1</sup>H NMR spectrum of, from top to bottom, BMC monomer, high-molecular-weight poly(TMC-co-BMC) and deprotected high-molecular-weight poly(TMC-co-BMC) (PTMC-OH). The copolymers contain 10 mol% of the functionalized BMC monomer. \* denotes the residual chloroform solvent signal. \*\* denotes water traces (from NMR solvent).

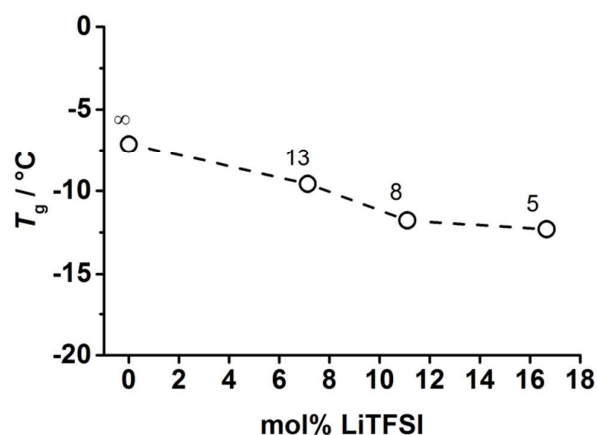


Figure 2. Glass transition temperature versus LiTFSI content for PTMC-OH-based electrolytes. The annotated numbers refer to the [carbonate]:[Li<sup>+</sup>] ratio.

of the polymers was confirmed with <sup>1</sup>H NMR as illustrated in Figure 1. The absence of the benzyl methylene signal at 4.48 ppm as well as the aromatic signals clearly revealed successful deprotection. In addition, the side group methylene signal shifted from 3.36 ppm to 3.48 ppm and shows a doublet splitting of 6.2 Hz in the deprotected polymer, thus indicating adjacency to the deprotected hydroxyl groups. Only very weak end-group methylene signals could be detected at around 3.7 ppm, indicating a number-average molecular weight well in excess of 100 000 g/mol, indicating that a high-molecular-weight copolymer was obtained in the polymerization and retained throughout the deprotection. GPC confirmed this and showed a slight decrease in *M<sub>n</sub>* from 329 000 g/mol to 271 000 g/mol when going from the Bn-protected polymer to PTMC-OH. This is not unexpected as, in a dilute solution, the hydroxyl groups of PTMC-OH will interact intramolecularly, leading to contraction of the polymer coil, which will give an

apparent lower molecular weight in GPC. This interpretation is in accordance with the polydispersity index being practically unaffected by the deprotection. From the hydroxyl-functional PTMC-OH, polymer electrolytes were prepared by blending the polymer host with LiTFSI salt. Through solvent casting, transparent, rubbery and mechanically stable films were obtained. DSC confirmed that the films were amorphous, which is a prerequisite for efficient ion transport.<sup>40, 41</sup> For typical polymer electrolytes, the ion mobility is directly coupled to the segmental motions of the polymer chains<sup>42</sup> which, in turn, is inversely related to the glass transition temperature (*T<sub>g</sub>*). Thus, for maximum ionic conductivity at a certain concentration of charge carriers, the *T<sub>g</sub>* of the material should be as low as possible. It should be noted that in this work a high molecular mobility, as indicated by a low glass transition temperature, was not specifically sought. Rather, the molecular interactions with a polar inorganic substrate were the main focus. As can be seen in Figure 2, the inclusion of 10 mol% of the hydroxyl-functional repeating unit in the polymer leads to a *T<sub>g</sub>* of -7.1 °C. While well below room temperature, this value is notably higher than for pure high-molecular-weight PTMC (*T<sub>g</sub>* = -16 °C<sup>19</sup>). This reduction of chain mobility is caused by intra- and intermolecular hydrogen bond interactions by the hydroxyl substituents in combination with hindered bond rotation because of the side groups. Of these effects, the interactions induced by the hydroxyl side groups are likely the major cause of the increase in *T<sub>g</sub>*, as indicated by the slightly lower *T<sub>g</sub>* of the benzyl ether-protected PTMC-co-BMC (*T<sub>g</sub>* = -10.6 °C), which has a bulkier side group (more hindered bond rotation) but lacks the hydrogen bond interactions. However, as indicated in Figure 2, when Li salt is added to the polymer matrix, the *T<sub>g</sub>* decreases with increasing salt content. This is in contrast to the PTMC-LiTFSI system as well as several other similar polycarbonate-based electrolyte systems where instead an increase in chain stiffness and *T<sub>g</sub>* is

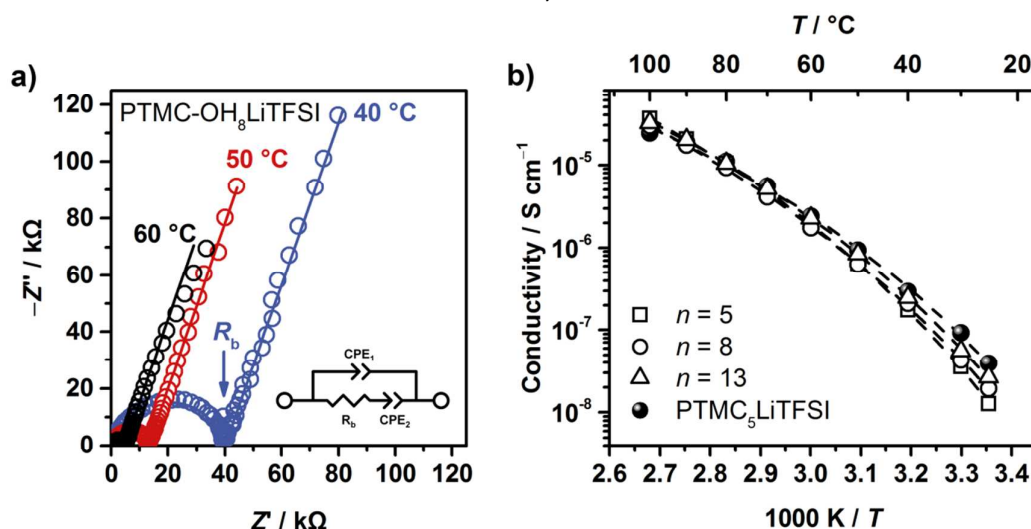


Figure 3. a) Nyquist plots of impedance data for PTMC-OH<sub>8</sub>LiTFSI at 40, 50 and 60 °C. Solid lines represent fits to an equivalent circuit (inset) used to obtain the bulk ionic resistance (*R<sub>b</sub>*). b) Arrhenius plot of total ionic conductivity versus temperature for hydroxyl-functional polycarbonate electrolytes with LiTFSI salt along with a PTMC<sub>5</sub>LiTFSI reference electrolyte. *n* refers to the [carbonate]:[Li<sup>+</sup>] ratio. Dashed lines represent Vogel-Tammann-Fulcher (VTF) fits.<sup>46</sup>

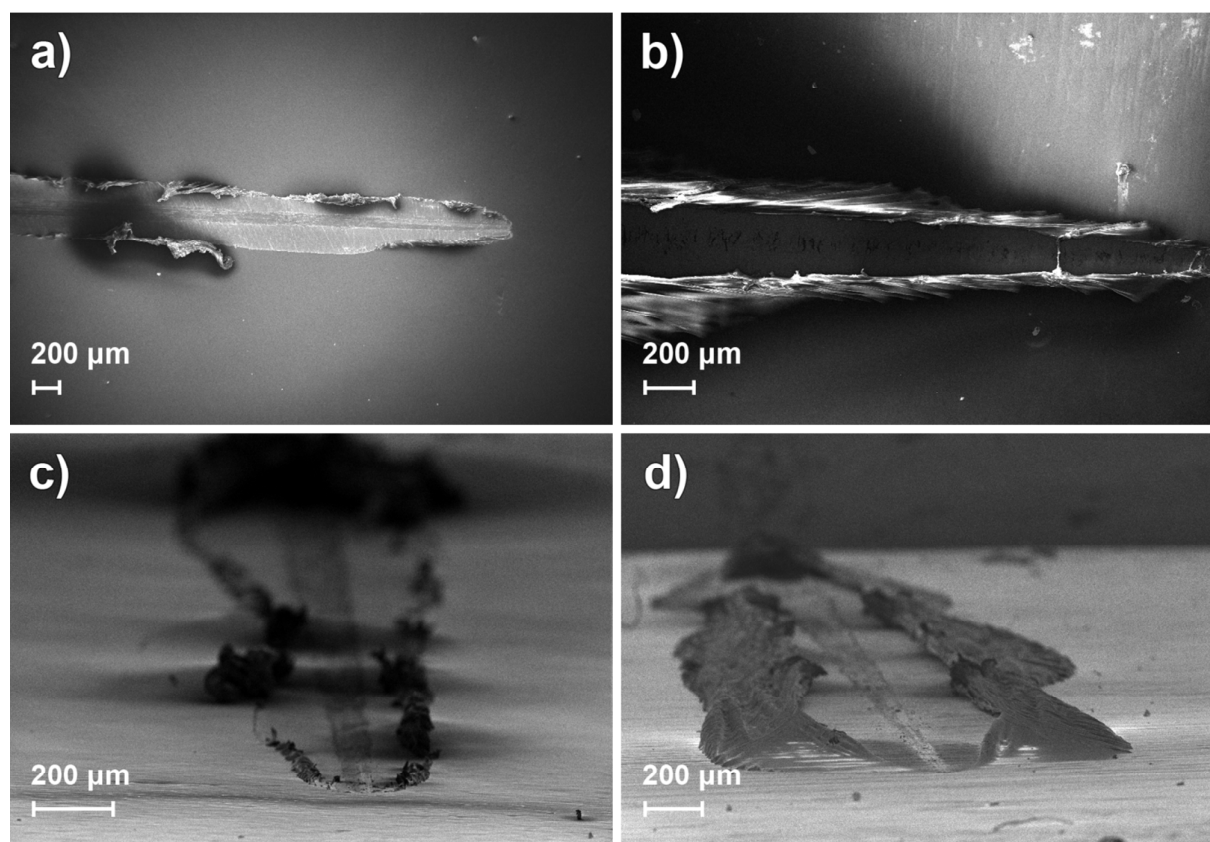


Figure 4. SEM images of scratch-tested polymer coatings on  $\text{TiO}_2$ -coated Ti substrates. a) PTMC-OH, top view; b) PTMC, top view; c) PTMC-OH, tilted view; d) PTMC, tilted view.

observed on addition of similar concentrations of LiTFSI due to  $\text{Li}^+$  coordination that creates transient crosslinks in the material.<sup>19, 21, 43</sup> A plausible explanation for this phenomenon is anion coordination. Whereas typical polymer electrolyte hosts can only coordinate to the cations of the salt, the hydroxyl groups of the present material can interact with the anions as well. This anion binding disrupts the hydrogen bonding interactions between hydroxyl groups, thereby cancelling out some of the stiffening effect of inter- and intramolecular interactions, leading to the observed decrease in  $T_g$ .

In order to determine the ion transport capabilities of the electrolytes, the total ionic conductivity of PTMC-OH-LiTFSI electrolyte films was determined through electrochemical impedance spectroscopy as presented in Figure 3. Quite unexpectedly, and in contrast to other polycarbonate electrolyte systems,<sup>19, 21, 43</sup> the ionic conductivity was found to be nearly independent on the salt concentration. Although not previously observed in our measurements on polycarbonate electrolytes, Armand *et al.* reported little variation with composition for PEO-LiTFSI electrolytes<sup>44</sup> and similar

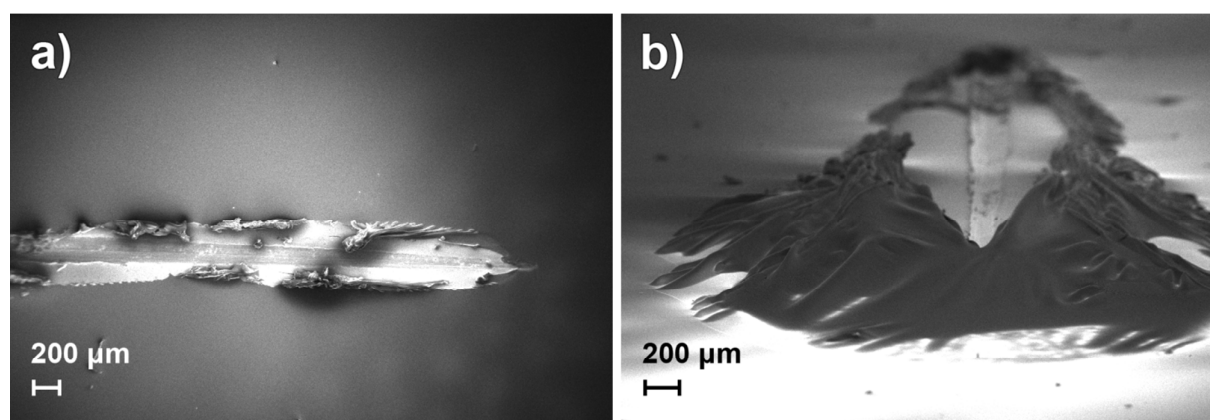


Figure 5. SEM images of scratch-tested polymer films on  $\text{Cu}_2\text{O}$ -coated Cu substrates. a) PTMC-OH, top view; b) PTMC, tilted view.

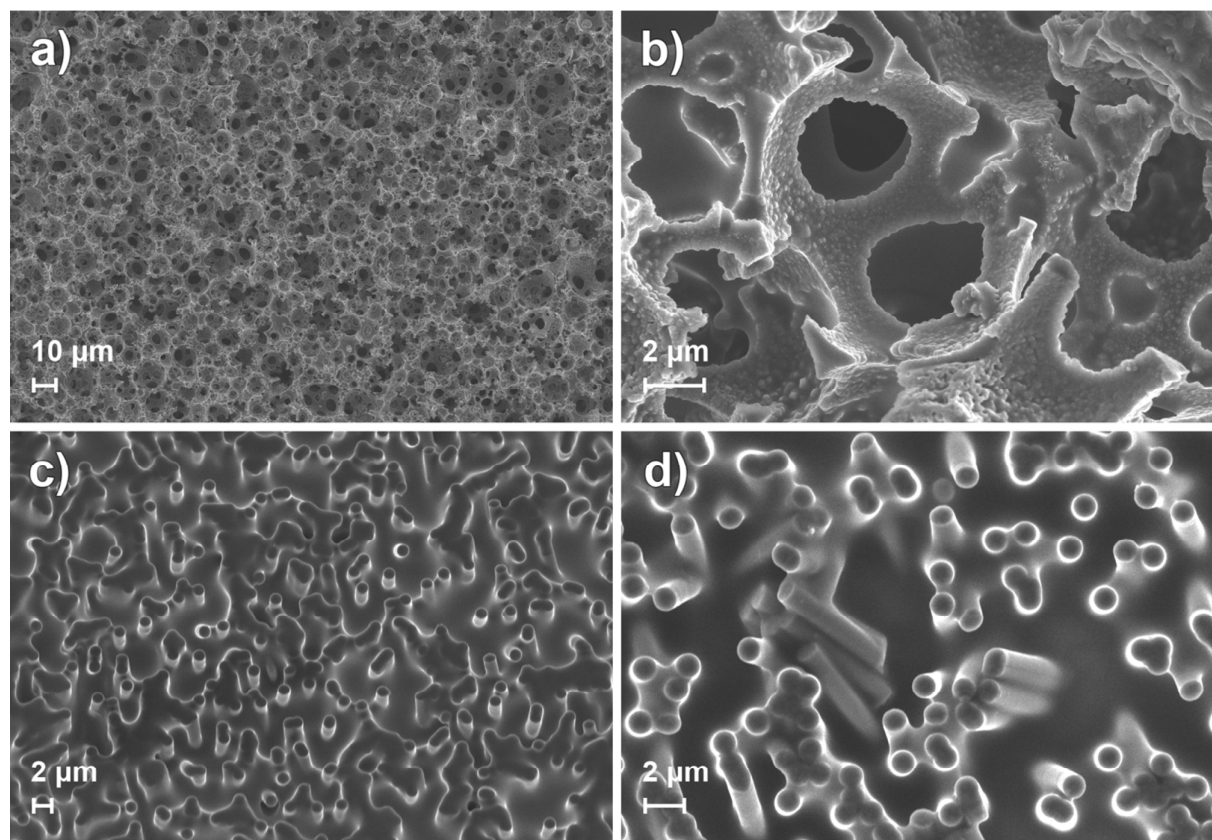


Figure 6. SEM images showing PTMC-OH/LiTFSI coatings on (a) and (b) LiFePO<sub>4</sub>-coated ultraporous carbon foam; (c) and (d) Cu<sub>2</sub>O-coated Cu nanopillars.

observations were also made by Forsyth *et al.* for poly(diethylene glycol carbonate)–sodium triflate electrolytes.<sup>45</sup> In the PTMC–OH system, this is possibly related to the same effect as the observed decrease in  $T_g$  with increasing salt concentration; *i.e.*, coordination of the TFSI anions to the hydroxyl groups of the polymer host, thus reducing anion mobility and partly offsetting the effect of higher ion concentrations on the total ionic conductivity. It is not unlikely that, at more extreme salt concentrations, a concentration-dependent ionic conductivity would indeed be observed. Furthermore, despite the higher glass transition temperatures, the total ionic conductivity of the PTMC–OH electrolytes was found to be similar to that of PTMC–LiTFSI electrolytes when determined using the same measurement setup (previous measurements on the PTMC–LiTFSI system, performed with a slightly different measurement protocol, tend to underestimate the conductivity at low temperatures).<sup>19</sup>

Although a reasonably high ionic conductivity is necessary for polymer electrolyte functionality, a more important issue for 3D-microbattery electrolytes is the ability form a thin, conformal coating on a 3D-structured electrode. Thus, the ability of the polymer to interact with the electrode surface and form a thin film with good surface adhesion is of prime importance. This was evaluated through scratch testing of PTMC and PTMC–OH films deposited on substrates consisting of either TiO<sub>2</sub> on Ti or Cu<sub>2</sub>O on Cu. Both these oxides are

relevant from a 3D-microbattery perspective for use as anode materials.<sup>6</sup> Cu<sub>2</sub>O is a conversion material that can be discharged reversibly through the reaction  $\text{Cu}_2\text{O} + 2\text{Li}^+ + 2\text{e}^- \rightarrow 2\text{Cu} + \text{Li}_2\text{O}$  with a reported capacity of up to 336 mAh g<sup>-1</sup> and a discharge potential of around 1.1 V.<sup>47</sup> TiO<sub>2</sub>, on the other hand, is an insertion material with a discharge potential of about 1.6–1.8 V and a capacity of up to 140 mAh g<sup>-1</sup>.<sup>48, 49</sup> The adhesion properties of the hydroxyl-functional polycarbonate on these materials were investigated through scratch testing on thermally oxidized Cu and Ti substrates and compared to the non-functionalized PTMC. As can be seen in Figure 4, the PTMC film shows clear delamination along the scratches on the TiO<sub>2</sub> substrate, indicating relatively poor adhesion. Such delamination was notably absent for the PTMC–OH film, confirming the ability of this material to beneficially interact with the polar metal oxide surface and provide good substrate adhesion. The same behavior was also observed on the Cu<sub>2</sub>O substrates (Figure 5). This shows that the hydroxyl functionalization, even at such a low concentration as 10% of the repeating units, is able to provide superior adhesion to electrode material surfaces.

For 3D-microbattery applications, the electrolyte needs to be deposited as a thin, uniform, conformal coating on 3D-structured electrode substrates and attaining such a coating is one of the major challenges in 3D-microbattery fabrication.<sup>4, 5, 16</sup> To properly address this, the investigation of the favorable interfacial interactions between the hydroxyl-functional PTMC-

OH and electrode surfaces was extended from 2D planar surfaces to 3D-microstructured electrodes by casting a PTMC-OH<sub>8</sub>LiTFSI electrolyte onto LiFePO<sub>4</sub>-coated ultraporous carbon foam<sup>29</sup> as well as Cu<sub>2</sub>O-coated Cu nanopillars.<sup>28</sup> These electroactive materials have shown promise for use as cathodes and anodes, respectively, in 3D-microbatteries. Figure 6 shows that a thin, conformal coating was obtained on both substrates. For the pristine substrates, please see Figure S2 and Figure S3, respectively, in the ESI. When paired with Li metal foils, OCV values of 3.0 V for the LiFePO<sub>4</sub>-coated carbon foam and 2.0 V for the Cu<sub>2</sub>O-coated nanopillars were measured, indicating that pinhole-free electrolyte layers were obtained that prevented the cells from short-circuiting. These results constitute a clear improvement over previously published results using a PTMC<sub>8</sub>LiTFSI electrolyte<sup>19</sup> and confirm the potential of utilizing hydrogen-bonding polycarbonates as electrolytes in 3D-structured battery assemblies.

## Conclusions

A high-molecular-weight aliphatic polycarbonate with hydroxyl side groups was synthesized and used to prepare Li<sup>+</sup>-conducting solid polymer electrolytes by adding LiTFSI salt to the polymer matrix. While these were found to be limited in ionic conductivity, this is not a crucial factor for the intended application in 3D-microbatteries where the ability to form a thin, conformal coating on a 3D-structured substrate is more important. Indeed, the introduction of the hydrogen bond-interacting hydroxyl groups, even at such a low concentration as 10 mol% of the repeating units, led to clear improvements in adhesion of polymer films to electroactive material substrates. Thin, conformal films could also be cast on 3D substrates in the form of LiFePO<sub>4</sub>-coated ultraporous carbon foam and Cu<sub>2</sub>O-nanopillars, thus showing that the favorable adhesion properties of PTMC-OH on 2D planar electrode substrates can be extended to 3D-microstructured battery electrodes as well. This confirms the suitability of the approach of using surface-active hydrogen-bonding groups as adhesion-enhancing functionalities in polymer electrolytes for 3D-microbatteries.

## Acknowledgements

This project was performed as part of the Ångström Advanced Battery Centre, funded by the Swedish Research Council (Grant No. 2012-4681). STandUP for Energy and The Carl Trygger Foundation are also acknowledged for financial support. In addition, the authors would like to acknowledge Maxim Galkin at the Department of Chemistry – BMC, Uppsala University, for assistance in the catalytic hydrogenation experiments, Magnus Heldin at the Department of Engineering Sciences, Uppsala University, for assistance with the scratch testing, Dr. Ulrica Edlund at Fibre and Polymer Technology, Royal Institute of Technology, for performing GPC measurements, and David Rehnlund and Habtom Desta Asfaw

at the Department of Chemistry – Ångström Laboratory, Uppsala University, for providing the 3D-battery electrodes.

## Notes and references

- 1 M. Armand and J. M. Tarascon, *Nature*, 2008, **451**, 652-657.
- 2 J. B. Goodenough and Y. Kim, *Chem. Mater.*, 2010, **22**, 587-603.
- 3 J. W. Long, B. Dunn, D. R. Rolison and H. S. White, *Chem. Rev.*, 2004, **104**, 4463-4492.
- 4 K. Edström, D. Brandell, T. Gustafsson and L. Nyholm, *Electrochem. Soc. Interface*, 2011, **20**, 48, 41-45.
- 5 M. Roberts, P. Johns, J. Owen, D. Brandell, K. Edstrom, G. El Enany, C. Guery, D. Golodnitsky, M. Lacey, C. Lecoeur, H. Mazor, E. Peled, E. Perre, M. M. Shaijumon, P. Simon and P.-L. Taberna, *J. Mater. Chem.*, 2011, **21**, 9876-9890.
- 6 M. Valvo, M. Roberts, G. Oltean, B. Sun, D. Rehnlund, D. Brandell, L. Nyholm, T. Gustafsson and K. Edström, *J. Mater. Chem. A*, 2013, **1**, 9281-9293.
- 7 C. P. Rhodes, J. W. Long, K. A. Pettigrew, R. M. Stroud and D. R. Rolison, *Nanoscale*, 2011, **3**, 1731-1740.
- 8 J. F. M. Oudenhoven, L. Baggetto and P. H. L. Notten, *Adv. Energy Mater.*, 2011, **1**, 10-33.
- 9 J. W. Fergus, *J. Power Sources*, 2010, **195**, 4554-4569.
- 10 V. Zadin and D. Brandell, *Electrochim. Acta*, 2011, **57**, 237-243.
- 11 G. El-Enany, M. J. Lacey, P. A. Johns and J. R. Owen, *Electrochem. Commun.*, 2009, **11**, 2320-2323.
- 12 B. Sun, D. Rehnlund, M. L. Lacey and D. Brandell, *Electrochim. Acta*, 2014, **137**, 320-327.
- 13 F. S. Teng, R. Mahalingam, R. V. Subramanian and R. A. V. Raff, *J. Electrochem. Soc.*, 1977, **124**, 995-1006.
- 14 D. Belanger and J. Pinson, *Chem. Soc. Rev.*, 2011, **40**, 3995-4048.
- 15 S. Tan, S. Walus, J. Hilborn, T. Gustafsson and D. Brandell, *Electrochem. Commun.*, 2010, **12**, 1498-1500.
- 16 S. Tan, S. Walus, T. Gustafsson and D. Brandell, *Solid State Ionics*, 2011, **198**, 26-31.
- 17 S. Tan, E. Perre, T. Gustafsson and D. Brandell, *Solid State Ionics*, 2012, **225**, 510-512.
- 18 B. Sun, I. Y. Liao, S. Tan, T. Bowden and D. Brandell, *J. Power Sources*, 2013, **238**, 435-441.
- 19 B. Sun, J. Mindemark, K. Edström and D. Brandell, *Solid State Ionics*, 2014, **262**, 738-742.
- 20 B. Sun, J. Mindemark, K. Edström and D. Brandell, *Electrochem. Commun.*, 2015, **52**, 71-74.
- 21 J. Mindemark, L. Imholt and D. Brandell, *Electrochim. Acta*, 2015, DOI: 10.1016/j.electacta.2015.01.074.
- 22 J. Mindemark and T. Bowden, *Polym. Chem.*, 2012, **3**, 1399-1401.
- 23 S. Venkataraman, N. Veronica, Z. X. Voo, J. L. Hedrick and Y. Y. Yang, *Polym. Chem.*, 2013, **4**, 2945-2948.
- 24 R. J. Ono, S. Q. Liu, S. Venkataraman, W. Chin, Y. Y. Yang and J. L. Hedrick, *Macromolecules*, 2014, **47**, 7725-7731.
- 25 G. S. Heo, S. Cho and K. L. Wooley, *Polym. Chem.*, 2014, **5**, 3555-3558.
- 26 W. Guerin, M. Helou, M. Slawinski, J.-M. Brusson, J.-F. Carpentier and S. M. Guillaume, *Polym. Chem.*, 2014, **5**, 1229-1240.
- 27 D. P. Sanders, D. J. Coady, M. Yasumoto, M. Fujiwara, H. Sardon and J. L. Hedrick, *Polym. Chem.*, 2014, **5**, 327-329.
- 28 M. Valvo, D. Rehnlund, U. Lafont, M. Hahlin, K. Edström and L. Nyholm, *J. Mater. Chem. A*, 2014, **2**, 9574-9586.
- 29 H. D. Asfaw, M. R. Roberts, C.-W. Tai, R. Younesi, M. Valvo, L. Nyholm and K. Edström, *Nanoscale*, 2014, **6**, 8804-8813.
- 30 C. Sisbandini, D. Brandell, T. Gustafsson and J. O. Thomas, *Electrochem. Solid-State Lett.*, 2009, **12**, A99-A101.

- 31 C. Sisbandini, D. Brandell, T. Gustafsson and L. Nyholm, *J. Electrochem. Soc.*, 2009, **156**, A720-A725.
- 32 E. M. E. Kristensen, F. Norder, H. Rensmo, T. Bowden, J. Hilborn and H. Siegbahn, *Langmuir*, 2006, **22**, 9651-9657.
- 33 Y. He, H. Keul and M. Möller, *React. Funct. Polym.*, 2011, **71**, 175-186.
- 34 T. F. Al-Azemi and K. S. Bisht, *Macromolecules*, 1999, **32**, 6536-6540.
- 35 R. F. Storey, B. D. Mullen and K. M. Melchert, *J. Macromol. Sci., Part A: Pure Appl. Chem.*, 2001, **38**, 897-917.
- 36 X. L. Wang, R. X. Zhuo, L. J. Liu, F. He and G. Liu, *J. Polym. Sci., Part A: Polym. Chem.*, 2002, **40**, 70-75.
- 37 Z. Xie, C. Lu, X. Chen, L. Chen, Y. Wang, X. Hu, Q. Shi and X. Jing, *J. Polym. Sci., Part A: Polym. Chem.*, 2007, **45**, 1737-1745.
- 38 A. P. Pêgo, D. W. Grijpma and J. Feijen, *Polymer*, 2003, **44**, 6495-6504.
- 39 D. J. Darensbourg, A. I. Moncada and S.-H. Wei, *Macromolecules*, 2011, **44**, 2568-2576.
- 40 E. Quartarone and P. Mustarelli, *Chem. Soc. Rev.*, 2011, **40**, 2525-2540.
- 41 K. P. Barteau, M. Wolffs, N. A. Lynd, G. H. Fredrickson, E. J. Kramer and C. J. Hawker, *Macromolecules*, 2013, **46**, 8988-8994.
- 42 M. A. Ratner and D. F. Shriver, *Chem. Rev.*, 1988, **88**, 109-124.
- 43 J. Mindemark, E. Törmä, B. Sun and D. Brandell, *Polymer*, 2015, **63**, 91-98.
- 44 M. Armand, W. Gorecki and R. Andréani, in *Proceedings of the Second International Symposium on Polymer Electrolytes*, ed. B. Scrosati, Elsevier Applied Science, London and New York, 1989, pp. 91-97.
- 45 M. Forsyth, A. L. Tipton, D. F. Shriver, M. A. Ratner and D. R. MacFarlane, *Solid State Ionics*, 1997, **99**, 257-261.
- 46 D. F. Shriver, B. L. Papke, M. A. Ratner, R. Dupon, T. Wong and M. Brodwin, *Solid State Ionics*, 1981, **5**, 83-88.
- 47 J. Y. Xiang, X. L. Wang, X. H. Xia, L. Zhang, Y. Zhou, S. J. Shi and J. P. Tu, *Electrochim. Acta*, 2010, **55**, 4921-4925.
- 48 S. Y. Huang, L. Kavan, I. Exnar and M. Grätzel, *J. Electrochem. Soc.*, 1995, **142**, L142-L144.
- 49 C. Natarajan, K. Setoguchi and G. Nogami, *Electrochim. Acta*, 1998, **43**, 3371-3374.